Communications Biology

https://doi.org/10.1038/s42003-026-09748-y

Article in Press

Manganese supplementation enhances cnidarian–dinoflagellate symbiosis under thermal stress

Received: 13 June 2025

Accepted: 13 February 2026

Cite this article as: England, H., Oakley, C.A., Herdean, A. *et al.* Manganese supplementation enhances cnidarian–dinoflagellate symbiosis under thermal stress. *Commun Biol* (2026). https://doi.org/10.1038/s42003-026-09748-y

Hadley England, Clinton A. Oakley, Andrei Herdean, David J. Hughes, Kittikun Songsomboon, Jennifer L. Matthews & Emma F. Camp

Manganese supplementation enhances cnidarian–dinoflagellate symbiosis under thermal stress.

Hadley England[1*], Clinton A. Oakley[2], Andrei Herdean[1], David J. Hughes[3], Kittikun Songsomboon[1], Jennifer Matthews[1], Emma F. Camp[1*]

*Corresponding Authors: hadley.england@uts.edu.au; emma.camp@uts.edu.au

1 University of Technology Sydney, Climate Change Cluster, Ultimo, NSW, 2007, Australia

2 Victoria University of Wellington, Wellington, 6012, New Zealand

3 National Sea Simulator, Australian Institute of Marine Science, Townsville, Qld, Australia

Abstract

Manganese (Mn) is an essential trace element for all photosynthetic life, playing an integral role in their photosystems, metabolism, and antioxidant activity. For corals, most studies focus on the potential toxicity of Mn at high concentrations (e.g. >700 µg L^{-1}). However, there has been less exploration on beneficial, biologically relevant levels of Mn. Combining promtomics, ICP, and PAM fluorometry, we evaluate how Mn supplementation at increasing concentrations (0.5, 4.8, 11.4, 15.6 µg L^{-1}) alters the physiology and proteome of the model cnidarian, *Exaiptasia diaphana*, when subjected to ambient (26 ˚C) and elevated (32 ˚C) temperatures. We demonstrate that Mn up to 15.6 µg L^{-1} mitigates thermal stress to *E. diaphana*, resulting in reduced photochemical damage and symbiont expulsion. Derived photobiology and proteomics data contributes to a mechanistic model for how Mn reduces thermal susceptibility, supporting the viability of Mn additions to enhance the protective capacities of photosynthetic cnidarians during heatwaves.

Introduction

Reef-building corals typically thrive in oligotrophic waters via efficient mechanisms and partnerships to retrieve nutrients from the water column [1]. For example, coral growth and health are supported through intricate relationships with associated symbionts, including receiving differing amounts of vitamins from bacteria [2] and photosynthetic products (glycerol, glucose, amino acids and lipids) from endosymbiotic dinoflagellates of the family Symbiodiniaceae [3–7]. Under optimal environmental conditions, photosynthetically fixed carbon is shared with the cnidarian host [8]; in return, the coral host provides the Symbiodiniaceae with a source of inorganic nutrients for photosynthesis and growth through various cellular and metabolic processes such as inorganic carbon (CO_2), ammonia (NH_3), and phosphate (PO_4^{3-}) [9]. However, when subjected to stress, this symbiotic partnership can breakdown, resulting in a loss of Symbiodiniaceae from the holobiont (a process known as bleaching; [10]), resulting in detrimental nutritional impacts for the cnidarian host, and the potential death of the organism if stressors persist for extended periods of time [11]. While several abiotic stressors (e.g. low salinity, cold exposure and disease) can cause coral bleaching, increasing seawater temperatures and more severe marine heat waves events are the primary cause of coral reef bleaching events [12].

Recent work has revealed that the abundance and stoichiometry of trace elements and nutrients are likely important factors contributing to the resilience of both the coral host [1,13] and its Symbiodiniaceae to stressors [14–16]. Manganese (Mn) is a particularly crucial element with diverse biological functions within both the ocean (where it is a limiting trace element in marine primary production [17,18]) and individual organisms due to its role in many essential physiological processes. As with other organisms, Mn is required by corals where it is an important cofactor of many enzymes, including the antioxidant enzyme Mn superoxide dismutase (Mn-SOD) which is an important ROS detoxifying enzyme for both the animal host and Symbiodiniaceae [13,19]. Additionally, Mn is required by all microalgae (such as Symbiodiniaceae), especially within the oxygen evolving complex (OEC), the first protein complex in the light-dependent reactions of oxygenic photosynthesis [14], which during thermal and light stress undergoes degradation and/or

upregulation of reactive oxygen species (ROS) [8]. Mn also plays a broader role in photoprotection and regulation [20] as well as aids in the maintenance of chlorophyll concentrations [13,14]. Additionally, Mn availability has been shown to impact macronutrient uptake and assimilation, phagocytosis, heterotrophy [21,22] and cell signalling [23,24]. However, despite the universal importance of certain trace elements, such as Mn, little research has been conducted to determine potentially beneficial concentrations of trace metals within reef systems [16], particularly when compared to relatively well-studied toxicological thresholds [25].

Mn typically exists in low concentrations (approx. 0.06 µg L^{-1}); [26] in the oligotrophic waters around coral reefs, but concentrations can exceed 7.54 - 11.12 µg L^{-1} in some areas [27,28]. At dramatically higher levels (e.g. 700 µg L^{-1}) Mn can be lethal to coral [29], and the Australian and New Zealand Environmental and Conservation Council (ANZECC) & Agriculture and Resource Management Council of Australia and New Zealand (ARMCANZ) (2000) provide a current guideline of 80 µg L^{-1} for Mn in marine waters. Sources of Mn contamination include mining, metal fabrication, herbicides, fossil fuels, and terrestrial runoff [29]. It has been demonstrated that intermittent (19.34 µg L^{-1}) and constant (4.1 - 4.24 µg L^{-1}) concentrations had a significant positive effect on coral thermal tolerance by maintaining photosynthetic rates under thermal stress[14,30]. Additionally, it was also shown that Mn positively impacted the cellular responses of corals to thermal stress through the decreased expression of heat shock proteins (HSPs) [13] as well as increased rates of calcification and photosynthesis [14]. However, it remains unknown if higher, constant levels of Mn (yet still below toxicological limits) can further benefit cnidarian-algal physiological performance, and what protein expression patterns support the maintenance of photosynthetic efficiency, optimum physiological functioning, and thus, symbiosis between both host and symbionts under stressful conditions. We therefore addressed these knowledge gaps using *Exaiptasia diaphana*, 'Aiptasia', as a model organism to study the effects of four different concentrations of Mn under both ambient and thermal stress conditions.

Much like common reef building corals, the sea anemone Aiptasia forms a symbiosis with Symbiodiniaceae. However, in contrast to corals, Aiptasia are easy to propagate in large numbers in laboratory environments [31], render symbiont-free (aposymbiotic, e.g.,[32], maintain genetic homogeneity, and manipulate the symbiont community [33]. Furthermore, a wealth of publicly

available data exists for Aiptasia, including its genome, proteome, metabolome, and transcriptome [5,34–36], leading to its wide acceptance as a model organism to study unique interactions of the cnidarian-algal symbiosis [37]. In this study we apply proteomic and photophysiological techniques to Aiptasia and hypothesize that differing concentrations of Mn affects the stability of both cnidarian symbiosis and photophysiology during thermal stress. Results from this study further our knowledge on the important role of Mn in Cnidarian symbiosis and its potential for use as an active reef intervention strategy.

Results

Symbiont Cell Densities

Symbiodiniaceae cell densities within all Aiptasia treatments held at 32ºC were generally lower than those held at 26ºC (ANOVA $F = 2.4$ and $p < 0.05$) (Fig. 1a), with the 0.5 µg L^{-1} Mn treatment at 32ºC being significantly (Tukey Post-hoc $p < 0.05$) lower (87%) than the control (0.5 µg L^{-1}) at 26ºC. Mn had a significant effect on cell densities under thermal stress (ANOVA $F = 4$ and $p < 0.05$) with Tukey Post-hoc revealing that the 15.6 µg L^{-1} treatment was significantly ($p < 0.05$) higher (370%) than 0.5 µg L^{-1} (Fig. 1a-c) (Supplementary Table 1) (Supplementary Data) Additionally, the 15.6 µg L^{-1} treatment at 32ºC experienced the smallest loss of symbionts (52%) relative to control. A moderate but significant correlation ($p < 0.05$, $R = 0.597$, Pearsons's rank test) between increasing Mn concentration and symbiont densities was evident for treatments at 32ºC, but not at 26ºC. Symbiont densities in control (0.5 µg L^{-1} at 26ºC) remined unchanged from the start of experiment (Supplementary Fig. 1) ($p > 0.05$, independent t test).

Photophysiology

All treatments (0.5, 4.8, 11.4 and 15.6 µg L^{-1}) at 32ºC exhibited lower maximum quantum yield of PSII (F_v/F_m) values relative to those at 26ºC (ANOVA $p < 0.05$) (Fig. 1d,e) (Supplementary Table 2) (Supplementary Data). However, addition of Mn increased F_v/F_m under the thermal stress treatment (Non-parametric Kruskal-Wallis test 9.611 $p < 0.05$ (ANOVA $F = 4.615$ $p < 0.05$) 0.296), but not at 26ºC (ANOVA $p > 0.05$). After 8 days at 32ºC, F_v/F_m values had dropped

24.2% for the 0.5 µg L^{-1} Mn treatment compared to an 8% decrease for the 15.6 µg L^{-1} Mn treatment (Fig. 1e). Mann-Whitney U tests indicated a significant difference ($p < 0.05$) between the lowest (0.5 µg L^{-1}) and three highest Mn treatments (4.8, 11.4 and 15.6 µg L^{-1}) when subjected to thermal stress. Overall, Mn addition therefore helped to maintain higher levels of photochemical efficiency under thermal stress whilst having no impact at 26ºC.

Proteomics

A total of 3970 host and 1515 symbiont proteins were detected. Differentially abundant proteins (DAPs) (limma FDR < 0.1, Log_2- Fold change > 0.25, < -0.25) were found between temperature treatments (26ºC vs 32ºC) and Mn concentrations at 32ºC (Fig. 2) but not at 26ºC. At 32ºC, lower Mn concentrations tended to have more DAPs than higher Mn concentrations compared to the control (0.5 µg L^{-1} 26ºC) for both host and symbiont (Fig. 2a-c). This is reflected in PCA plots (Fig. 2a,b) where higher Mn treatments at 32ºC form clusters closer to those at 26ºC. In particular, the 11.4 µg L^{-1} and 15.6 µg L^{-1} treatments at 32ºC for the symbiont proteome appeared to cluster together closer to those at 26ºC than the lower Mn concentrations. PERMANOVAs were conducted where it was shown that both the symbiont ($F = 4.02$, $R = 0.54$ and $p < 0.05$) and host ($F = 3.07$, $R = 0.47$ and $p < 0.05$) proteome were significantly affected by the addition of Mn under thermal stress.

Host Proteome

One DAP was found between the Mn treatments at 32ºC, however temperature (26ºC vs 32ºC) had a significant effect with 175 DAPs (Limma FDR < 0.1 Log_2- Fold change > 0.25, < -0.25) observed between 0.5 µg L^{-1} treatments. HSP 90 alpha-1 and HSP71 were significantly (Limma FDR < 0.1 Log Fold change > 0.25, < -0.25) up-regulated in 0.5 µg L^{-1} Mn at 32ºC treatments compared to those at 0.5µg L^{-1} Mn at 26ºC (control), with higher Mn treatments being closer to control levels (Supplementary Table 3).

Symbiont Proteome

At 32ºC a total of 24 DAPs were observed between the highest (15.6 µg L^{-1}) and lowest (0.5 µg L^{-1}) Mn treatments in the symbiont proteome (Fig 2a,b). DAPs between 32ºC treatments (0.5 – 15.6 µg L^{-1}) in the symbiont proteome consisted of photosynthesis, energy metabolism, protein

folding and stress response related proteins (Fig. 3a,b). Heat shock protein (HSP) levels in the symbiont (Fig. 3c) were elevated under thermal stress. Interestingly, treatments with the highest Mn concentration (15.6 µg L^{-1}) displayed elevated levels of HSPs compared to the lowest Mn treatment (0.5 µg L^{-1}) (Supplementary Table 4).

Gene Enriched Ontology

Gene ontology (GO) analysis was subsequently performed to further understand how treatments influenced the physiological functioning of the Aiptasia. Enriched GO terms (Limma FDR < 0.1, Log_2- Fold change > 0.25, < -0.25) were compared for both the host and symbiont between control (0.5 µg L^{-1} at 26ºC) and treatments (0.5 µg L^{-1} and 15.6 µg L^{-1} at 32ºC)(Supplementary Tables 5 and 6), as well as between treatments at 32ºC (0.5 µg L^{-1} and 15.6 µg L^{-1}) for the symbiont. GO terms were sorted into the three main ontologies, "biological processes" (BP), "cellular compartment" (CC) and "molecular function" (MF) with clear differences in both up and down regulated GO term classifications being identified between 0.5 µg L^{-1} and 15 µg L^{-1} treatments at 32ºC within the symbionts. The addition of Mn during thermal stress had a significant (Limma FDR < 0.1, Log_2- Fold change > 0.25, < -0.25) impact on the abundance and type of enriched GO terms from the symbiont but not the host. For the symbiont, when comparing the 15.6 µg L^{-1} treatment to the 0.5 µg L^{-1} treatment at 32ºC, 23 up and 10 down regulated GO terms were identified.

In the host, zero enriched GO terms were observed between Mn treatments, but were present between control and elevated temperatures (26 ºC and 32ºC). GO Terms between 0.5 µg L^{-1} treatments consisted of protein folding and structural modification as opposed to the 15.6 µg L^{-1} treatment at 32ºC (compared to control) which included detoxification terms (Supplementary Table 6).

Table 1. Gene ontology **(**GO) terms enriched (Limma FDR < 0.1, Log_2- Fold change > 0.25, < -0.25) between 0.5 µg L^{-1} and 15 µg L^{-1} treatments at 32ºC for algal symbionts**.**

		Up Regulated	
GO ID	***GO TERM***	***DAPS***	***P VALUE***
Biological Process			
GO:0006457	protein folding	4	0.014
	oxaloacetate	1	
GO:0006107	metabolic process		0.022

GO:0005977	glycogen metabolic process	1	0.043
GO:0006011	UDP-alpha-D-glucose metabolic process	1	0.043
GO:0042549	photosystem II stabilization	1	0.064
GO:0006099	tricarboxylic acid cycle	2	0.080
GO:0015977	carbon fixation	1	0.085
GO:2001295	malonyl-CoA biosynthetic process	1	0.085
Cellular Compartment			
GO:0019898	extrinsic component of membrane	1	0.037
GO:0009654	photosystem II oxygen evolving complex	1	0.055
Molecular Function			
GO:0140662	ATP-dependent protein folding chaperone	4	0.0010
GO:0005524	ATP binding	8	0.0013
GO:0051082	unfolded protein binding	3	0.0076
GO:0008964	phosphoenolpyruvate carboxylase activity	1	0.0174
GO:0003994	aconitate hydratase activity	1	0.0174
GO:0047456	2-methylisocitrate dehydratase activity	1	0.0174
GO:0003983	UTP:glucose-1-phosphate uridylyltransferase activity	1	0.0345
GO:0003989	acetyl-CoA carboxylase activity	1	0.0513
GO:0004222	metalloendopeptidase activity	1	0.0513
GO:0016887	ATP hydrolysis activity	3	0.0525
GO:0042132	fructose 1,6-bisphosphate 1-phosphatase activity	1	0.0679
GO:0043531	ADP binding	1	0.0679
GO:0004807	triose-phosphate isomerase activity	1	0.0841

Down Regulated

GO ID	***GO TERM***		***P VALUE***
Biological Process			
GO:0090385	phagosome-lysosome fusion	1	0.0051
GO:0008333	endosome to lysosome transport	1	0.0051
GO:0000045	autophagosome assembly	1	0.0101
GO:0046907	intracellular transport	2	0.0600
Cellular Compartment			
GO:0005770	late endosome	1	0.0051
GO:0005764	lysosome	1	0.0204
GO:0045335	phagocytic vesicle	1	0.0204
GO:0030076	light-harvesting complex	1	0.0255
Molecular Function			

GO:0003924	GTPase activity	2	0.0052
GO:0005525	GTP binding	2	0.0055

Superoxide Dismutase Abundance

SOD abundances were similar across all treatments (temperature andMn) for the host when compared to control levels (0.5 µg/L^{-1} at 26ºC). However, in the symbiont, SOD abundance was significantly (Limma FDR < 0.1, Log_2- Fold change > 0.25, < -0.25) lower for 0.5, 4.8 and 11.4 µg/L^{-1} Mn treatments at 32ºC compared to control (0.5 µg/L^{-1} at 26ºC), whilst the 15.6 µg/L^{-1} Mn treatment at 32ºC maintained abundances of SOD similar to controls.

Discussion

Trace elements are vital for the optimal functioning of many ecosystems [16,38], particularly coral reefs, where essential elements such as Mn are often found in very low concentrations [27]. Research into trace elements to date has primarily focused on toxicity [25] with few studies examining beneficial concentrations of these elements and what effects elevated and/or depleted concentrations may have on coral reef taxa [16]. We therefore investigated the effects of varying non-toxic Mn concentrations on the model cnidarian *Exaiptasia diaphana* and its symbiotic microalgae, *Breviolum minutum*, revealing how even small additions in Mn concentration has the capacity to increase their thermal tolerance.

Maintenance of photochemical efficiency and symbiosis under manganese additions

In alignment with previous studies [13,14], Aiptasia maintained higher values of F_v/F_m with the addition of Mn under thermal stress, however contrary to these studies, our results indicated that Mn addition maintained algal symbiont densities (Fig. 1a,d) (Supplementary Tables 1 and 2), suggesting that Mn can protect and/or enhance fundamental photophysiological processes required for the transfer of nutrients and ultimate maintenance of symbiosis between algae and host. This maintenance of symbiosis aligns with previous studies that have shown thermally damaged symbionts with low F_v/F_m were expelled from the host whilst those with higher F_v/F_m were maintained [39]. Therefore the addition of Mn has the potential to mitigate the impacts of thermal stress in cnidarians, together with enhancing the efficiency and protection of the photosystems within their algal symbionts [13,14]. Similar effects have also been reported in other

photosynthetic organisms, where Mn boosts the efficiency and protection of the oxygen evolving complex (OEC) in PSII [20,40–42]; this is important as the OEC is often the first target of thermal stress in Symbiodiniaceae [43,44]. We found that concentrations of Mn between 4.8-15.6 µg L^{-1} had a beneficial impact, helping to maintain photochemical efficiencies under thermal stress (Fig. 1) (Supplementary Table 1). F_v/F_m values in the two lowest Mn concentrations at 32ºC generally declined over time with increased exposure to thermal stress, however Aiptasia maintained in 4.8 µg L^{-1} of Mn experienced a sudden increase in F_v/F_m (Fig. 1e) on the penultimate day of the experiment. Interestingly, this sudden 'recovery' of photochemical efficiency coincided with an increase in the rate of symbiont expulsion, suggesting photosynthetic efficiency was potentially increased due to reduced competition for Mn among remaining algal symbionts within the host, aligning with findings of previous studies [13,14,38]. The effects of different Mn concentrations were further demonstrated by Iyagbaye et al., (2022) where host and symbiotic algae appear able to partition Mn when exposed to higher concentrations, with the symbiont maintaining a higher concentration than the host tissue [45].

Manganese has a significant effect on the proteome of the Symbiodiniaceae of Aiptasia under thermal stress

Consistent with prior studies [46] temperature exerted a pronounced effect on the proteomes of both the host and symbionts (Fig. 2a,b). Mn treatments impacted symbionts but not host, suggesting that Mn addition plays a crucial role in preserving the proteostasis of the algal symbiont under thermal stress. Both unique and shared GO terms were identified between 0.5 µg L^{-1} and 15.6 µg L^{-1} Mn treatments at 32ºC, indicating that whilst some processes were common across treatments, Mn addition induced treatment specific changes in the proteome. Enriched GO terms from the symbionts under thermal stress were consistent with those from other studies where terms relating to PSII, protein folding and energy metabolism were all impacted by elevated temperature. Terms such as 'Photosystem II stabilisation' and 'Photosystem II oxygen evolving complex' were enriched with Differentially abundant proteins (DAPs) under thermal stress at 0.5 µg L^{-1} but not at 15.6 µg L^{-1} Mn (Supplementary Table 1) compared to control (26ºC), corresponding with F_v/F_m results where treatments at 32ºC with higher Mn concentrations exhibited greater photochemical efficiencies, suggesting that PSII capacity was enhanced by Mn availability. Additionally, GO terms related to protein folding, energy

metabolism and other enzymatic activities were enriched between 0.5 µg L^{-1} and 15.6 µg L^{-1} Mn treatments under thermal stress (Table 1), indicating that downstream metabolic processes were able to be maintained.

Under thermal stress, only one DAP was found between Mn treatments for the host, however 24 DAPs were observed in the symbiont proteome between the lowest (0.5 µg L^{-1}) and highest (15.6 µg L^{-1}) Mn concentrations. Interestingly, changes to PSII appeared to be limited to extrinsic proteins with no differences found between intrinsic and core PSII proteins such as D1 and D2 – perhaps partly due to the ability of D1/D2 to be continuously repaired [20]. Photosynthetic proteins such as 'PS II 12kDa', 'Psb31', 'SBPase' and 'Cytochrome C_{550}' were significantly downregulated under thermal stress at 0.5 µg L^{-1} when compared to the 15.6 µg L^{-1} treatment (Limma FDR < 0.1, Log_2- Fold change > 0.25, < -0.25). Generally, protein abundances at 15.6 µg L^{-1} Mn (32ºC) were much closer to those seen under ambient conditions (0.5 µg L^{-1} Mn, 26ºC) (Fig. 3a), again suggesting higher levels of Mn helped to maintain functional photosynthetic machinery, particularly the oxygen evolving complex (OEC), as with previous work [20,41] that showed Mn limitation can significantly disrupt the functionality of PSII. Several proteins either incorporate Mn in their functions or work directly in the OEC [47]. For example, extrinsic proteins such as cytochrome C_{550} and PS II 12 kDa (PsbU) stabilise the OEC by protecting the Mn cluster from external reductants [48,49] and the presence of PS II 12kDa (PsbU) in *Synechococcus* sp. increased the thermal stability of the OEC [50,51]; in the latter case where PsbU may afford protective ability against ROS [52]. However, little is known about the role of Psb31 in higher plants and algae, although limited research suggests Psb31 can serve as a substitute for the Mn stabilising protein – PsbO – in marine diatoms [53]. We observed significant downregulation of these extrinsic proteins (C_{550}, PsbU and Psb31), accompanied by no measurable changes in D1and D2 protein expression and reduced photochemical efficiencies (F_v/F_m) at 32º C and limiting Mn conditions (0.5 µg L^{-1}) when compared to higher Mn treatments (15.6 µg L^{-1}, 32º C), suggesting declining photosynthetic capacity may be caused by accumulation of damaged or non-functional OECs.

Other DAPs such as aconitate hydratase B, AtpH protein, acetyl-CoA carboxylase and phosphoenolpyruvate carboxylase represent enzymes involved in metabolic processes such as the

Krebs cycle, ATP synthesis, fatty acid metabolism and carbon fixation. All four of these proteins were downregulated in low Mn concentrations (0.5 µg L^{-1}) under thermal stress (32ºC) when compared to higher Mn levels (11.4-15.6 µg L^{-1}) which showed similar expression rates as Aiptasia kept at 26ºC (all Mn treatments) (Limma FDR < 0.1, Log_2- Fold change > 0.25, < -0.25) (Fig. 3a). Such responses further indicate that these downstream metabolic processes were maintained or enhanced from more efficient photosystem functioning under Mn addition. We also observed upregulation of Rab-7a in our thermally exposed Aiptasia, particularly in lower Mn treatments (0.5 µg L^{-1}) where expression rates were significantly higher than those exposed to increased levels (15.6 µg L^{-1}) of Mn. Proteins such as Rab-7a (and YPT1) are likely key regulators of vesicular trafficking and are thought to play a direct role in the maintenance of cnidarian-algal symbiosis through phagocytosis [54,55]. Healthy symbionts appear to be able to reject the host derived Rab-7a proteins whilst thermally damaged and photosynthetically impaired algal cells carried this protein [54,55]. Interestingly Rab-7a was not detected in over half of the Aiptasia at 26ºC thereby supporting previous work that healthy symbionts were less likely to carry this protein.

Overall, heat shock protein (HSP) expression levels were elevated across both host and symbionts at 32ºC (all Mn treatments) when compared to 26ºC treatments (Fig 2c) (Supplementary Fig. 1). Contrary to the host, HSP levels in the symbiont were elevated by addition of Mn under thermal stress, with HSP 90 being significantly higher (Limma FDR < 0.1, Log_2- Fold change > 0.25, < -0.25) in the 15.6 µg L^{-1} treatment compared to 0.5 µg L^{-1} (Fig. 3c). As such, whilst photosynthetic efficiency was higher under elevated Mn (as shown in Fig 3) algal cells may be experiencing a higher demand for protein repair and maintenance processes (Fig. 3c) thereby resulting in higher HSP expression amongst Mn-treated Aiptasia under thermal stress. Both Biscéré et al. (2018) and Montalbetti et al. (2021) previously showed that corals subjected to increased Mn concentrations exhibit higher thermal tolerance, but no change in SOD activity [13,14]. This is interesting as current leading theories suggest that that cofactors and enzymes such as SODs play a vital role in the suppression of ROS-induced bleaching. However, similar to previous studies, we observed no significant up-regulation in SOD expression (Fig.5) as a result of either heat stress [56] or Mn treatments [13]. Consequently, SOD activity is likely saturated resulting in greater cellular damage from ROS [56] increasing the rate of required repair

and folding from HSPs. It has also been shown that HSPs such as Dnak2 can both directly and indirectly support PSII function through the facilitation of protein import, stabilisation and folding in the thylakoid membrane [57,58]. The fact that HSP expression levels were reversed for high and low Mn treatments (0.5 µg L^{-1} vs 15.6 µg L^{-1} at 32ºC) in the host versus symbiont indicates that although under Mn enrichment the symbiont is exhibiting greater stress responses through elevated HSP expression, it can maintain a better partnership with the host, indicated by lower host HSP expression.

Photosystem II inhibition and repair

Under normal conditions, PSII is in a constant state of damage and repair, with reassembly of the OEC occurring as often as every 15–30 minutes [40]. However, increased light and thermal energy can impact the rate of damage and thus, the rate of required PSII reassembly [59]. Interestingly, the rate of OEC reassembly, especially the Mn_4Ca cluster, is heavily dependent on cellular concentrations of available Mn^{2+} [40]. As PSII breaks down, oxidised Mn ions are lost from the OEC and, without access to free Mn^{2+}, OEC reassembly is inhibited, thus impairing photochemistry and downstream metabolic pathway activity within the symbiont. A drop in photosynthetic metabolic activity inherently reduces the ability of the cell to function and repair, including HSP production [60] (Fig. 3c) . This was shown in the 0.5 µg L^{-1} Mn treatment at elevated temperature (32ºC), where photochemical efficiency, extrinsic protein and HSP abundances were all reduced compared to higher Mn concentrations.

Our proposed metabolic cascade from Mn limitation would reduce the amount of resource sharing with the host and the ability of the algal cell to fend off host derived RAB-7a proteins which are a marker for phagocytosis [54,55], ultimately ending in bleaching (Fig. 1b) (Supplementary Fig 2). The results from our study as well as those of [13] support this hypothesis, as we observed no significant increases in SOD expression above control levels (0.5 µg/L^{-1} at 26ºC) (Fig. 4) across Mn treatments at 32ºC but significant upregulation of HSPs, extrinsic proteins and metabolic/energy production proteins, as well as a down regulation in RAB-7a and YPT1 in high Mn treatments. Further to this, higher expression of Psb31, a known substitute for PsbO (Mn-stabilising protein) was observed, indicating that the OEC repair processes were active whilst still maintaining reasonable functionality. Should this theory be incorrect and SOD

did in fact scavenge excess ROS in higher Mn-treated Aiptasia, a reduction of HSP levels alongside an increase in SOD compared to control (0.5 µg/L^{-1} at 26ºC) levels should have been observed, however this was not the case. It was observed in the symbionts under thermal stress that concentrations of 15.6 µg/L^{-1} prevented any significant (limma FDR < 0.1, Log_2- Fold change > 0.25, < -0.25) decline in SOD activity compared to the control (0.5 µg/L^{-1} at 26ºC), however SOD levels were still well below those kept at 26ºC, indicating that levels of SOD were declining due to the breakdown of other cellular activities and did not increase in line with theorised increases of ROS.

Despite this, the generation of ROS under thermal stress is known to induce intra and extracellular damage, causing metabolic cascades that play an important role in the breakdown of cnidarian-algal symbiosis. However results from both this and previous studies show that it may not be the sole primary cause of holobiont dysregulation [8,11,61]. Data here suggests an additional plausible explanation being that the breakdown of the host-symbiont relationship is linked closely to the ability of the algal symbionts to maintain metabolic functioning through continued photosynthetic efficiency, thus maintaining their ability to share metabolites with the cnidarian host.

It is also important to note that there are many other SOD independent mechanisms for scavenging ROS (catalase, peroxidases, peroxiredoxins and other non-enzymatic antioxidants [62]) that may have played a role in the mitigation of thermal stress. However, our results did not identify any significant differences in their abundances under the conditions tested. Additionally, recent research [8,11,61,63,64] has raised questions about whether ROS is the primary driver of bleaching, suggesting that other processes such as metabolic dysfunction or impaired nutrient cycling may play a more central role. While the ROS model remains widely accepted, these alternative mechanisms warrant further investigation to better understand the complex factors contributing to holobiont breakdown during thermal stress.

Other influences of Manganese

In eukaryotes Mn is vital for mitochondrial ATP synthesis and regulation [65,66] where Mn-dependant enzymes such as pyruvate carboxylase, arginase and Mn-SOD rely on free Mn^{2+} ions to carry out and maintain key metabolic functions [67]. Limited information exists on its role within marine taxa but in other organisms Mn is known to substitute/compete with ions such as

Mg^{2+} and Ca^{2+} for binding sites where it can influence mitochondrial function and energy metabolism [68]. To date, little to no research has been conducted on corals that combines Mn enrichment and omics analysis, and while we observed no significant proteomics-based changes in these enzymes and proteins this does not imply that low-level Mn enrichment affects PSII only.

Conclusion

Photosynthetic organisms underpin the existence of modern coral reefs yet are extremely sensitive to environmental changes such as ocean warming. It is therefore important to identify ways in which photosynthetic organisms can both be protected and enhanced as effects of climate change increase. Here, we show that maintenance of photosynthetic efficiency and photosynthetic metabolism under thermal stress is strongly linked to the availability of Mn, with increases in the trace metal directly correlating to enhanced photochemical efficiency and overall holobiont function. This study not only provides empirical evidence on the benefits of increased exogenous Mn availability during thermal stress in cnidarians but is also the first to characterise its effects at both the physiological and proteomic level in the holobiont. Despite the novelty of this study, future experiments could benefit from additional data such as OJIP analysis and host/symbiont elementomics to help paint a clearer picture on the effect of Mn supplementation. This study provides foundational knowledge that paves the way for future work and the potential use of Mn supplementation in situ during periods of thermal stress, with the aim of supporting and increasing the resilience of coral reefs amidst the backdrop of climate change.

Methods

Experimental setup

Symbiotic *Exaiptasia diaphana* (AIMS 3 genotype) (herein called Aiptasia) were sourced from the Australian Institute of Marine Science (AIMS, Townsville, Qld, Australia) and its Symbiodiniaceae was identified as *Breviolum minutum* [34]. Aiptasia were grown in 500 mL glass containers held in a water bath maintained at 26 ± 0.3ºC by Inkbird thermostats (INKBIRD Tech.

C.L, China). Lighting consisted of Hydra 52s (Aqua illumination, USA) providing 50 µmol photons m^{-2} s^{-1} of light on a 12:12 light/dark cycle (representative of their natural environments). Aiptasia were grown in custom artificial seawater (35 ppt), comprised of a salt solution with a modified L1 trace component (Supplementary Tables 7 and 8) that was replenished in each tank at a rate of 1000 mL day^{-1} via Red Sea peristaltic pumps (Red Sea Aquatics, Israel). The modified L1 trace component mix (Supplementary Tables 7 and 8) was designed to represent oligotrophic reef conditions and allow for element specific manipulations. Media was freshly made every other day and tested via inductively coupled plasma mass spectrometry (ICP-MS) (Supplementary Table 9; see methods below). Aiptasia were fed *Artemia* nauplii (instar 1) twice a week (also grown in the modified media) and following feeding the tanks were cleaned to minimise algal growth. Aiptasia were propagated and genetic homogeneity was maintained by cutting them in half when their oral disks reached a diameter of ca. 6-7 mm, and subsequently were left to regrow [31].

The experimental setup consisted of four water baths, two maintained at a temperature of 26 ± 0.3ºC and two that were incrementally temperature ramped to 32 ± 0.3ºC at a rate of 0.5ºC per day over 12 days. Each water bath contained four 500 mL glass containers, one for each Mn concentration (0.5 ± 0.2, 4.8 ± 0.5, 11.4 ± 0.8 and 15.6 ± 0.6 µg L^{-1}), resulting in a total of eight experimental treatments: 26ºC 0.5 µg L^{-1} (control), 26ºC 4.8 µg L^{-1}, 26ºC 11.4 µg L^{-1}, 26ºC 15.6 µg L^{-1}, 32ºC 0.5 µg L^{-1}, 32ºC 4.8 µg L^{-1}, 32ºC 11.4 µg L^{-1}, 32ºC and 15.6 µg L^{-1}. Modified seawater was delivered to each corresponding container at a rate of 500 mL every 12 hours via a peristaltic pump (Red Sea Aquatics, Israel). Sixteen Aiptasia measuring 5-6 mm were placed into each 500 mL container. Two water baths were then ramped up in temperature from 26ºC to 32ºC at a rate of 0.5ºC per day using controllable thermostats (Inkbird, Australia) and titanium heaters (Schego, Germany). The water baths were then held at this temperature for eight days, until a drop of ca. 30% in values of maximum PSII photochemical efficiency (F_v/F_m) was observed in Aiptasia kept in 0.5 µg L^{-1} of Mn. This was done to ensure that samples would contain enough symbionts for proteomics analysis as well as maintaining as many photosynthetically damaged symbionts as possible before they are expelled from the host.

PAM fluorometry

Maximum photosystem II (PSII) efficiency (F_v/F_m) was determined after a 20-minute period of dark acclimation using a Waltz Diving PAM (Heinz Walz Gmbh, Germany). Measurements were performed every second day until the end of the ramping period, and then daily until the end of experiment between the hours of 12-1 pm. To ensure stray light from the Diving-PAM fluorometer did not affect the dark acclimation of other Aiptasia, individuals were placed into smaller 10 mL wells within the same water baths prior to being measured. A 10 mm spacer was utilised on the end of the fibre optic sensor to maintain a standardised distance between the fibre optic and Aiptasia for each measurement performed. The fibre optic was placed above the centre of each Aiptasia ensuring that the whole organism was captured each measurement with a total of eight Aiptasia measured for each treatment.

ICP-MS analysis

Water samples from each new batch of media were tested for Mn using an Agilent 7700, ICP-MS (Agilent, USA) (Supplementary Table 9). Samples were placed into the SPS 4 autosampler MS (Agilent, USA), the sampling tip was rinsed, and the system purged using 2% nitric acid between samples for 30 seconds. To minimise machine drift and build-up of salt within the machine, an argon humidifier (PerkinElmer, USA) was used, and samples were diluted to 1:5 in a 2% ultra-pure nitric acid solution (Seastar, Canada). Rhodium and yttrium were used as internal standards and calibration curves (0, 1, 2, 4, 8, 16 and 32 µg L^{-1}) were created using a 20 component, ICP-MS standard at 10 µg L^{-1} in 2% HNO_3 + Tr HF (ZeptoMetrix, USA). Spike recoveries were performed by adding 10 µg L^{-1} of Mn to four randomised samples at the end of each run to verify that limited machine drift occurred. Blanks and calibration curves were matrix matched using high purity analytical grade chemicals (Sigma Aldrich, Germany) (Supplementary Table 10).

Proteomic analysis

Aiptasia were processed similar to Oakley et al. [46]. Frozen Aiptasia were washed in 1 mL HPLC-grade water to remove salts before being mechanically homogenised with a Dounce homogeniser in 500 µL HPLC-grade water. The microalgal fraction was separated by low-speed centrifugation (Eppendorf 5424 microcentrifuge) (200 *g* × 30 seconds) and the supernatant,

containing host protein, was transferred to a new tube. The algal pellet was frozen at −80 °C until later processing with the same method. The host protein was denatured by addition of sodium deoxycholate to a final concentration of 5% w/w, with 100 mM triethylammonium bicarbonate buffer (TEAB, pH 8.5), and 10 mM tris (2-carboxyehtyl) phosphine (TCEP) as a reductant. Samples were incubated at 90−95 °C for 20 minutes and then disrupted using an ultrasonicator probe (20 × 2 second pulses) to lyse cells and to denature and dissolve proteins. Lipids and pigments were reduced by an ethyl acetate phase transfer, where the sample was agitated with 1 mL ethyl acetate for 1 minute, followed by centrifugation (10,000 *g* × 1 minute). The upper, ethyl acetate layer was removed and the process repeated before the residual ethyl acetate was removed by centrifugation under vacuum for 15 minutes. The remaining aqueous protein sample was transferred to a 0.5 mL 30 kDa molecular weight cutoff filter (Amicon Ultra, Merck Millepore) for filter-aided sample preparation [69]. Each protein sample was concentrated in the filter by centrifugation (14,000 *g* × 20 minutes), resuspended in 380 µL 100 mM TEAB in the filter, centrifuged again, and the process repeated before resuspending the sample in 400 µL 100 mM TEAB. A 10µL subsample was acidified and pelleted to remove deoxycholate, then the protein quantified (Qubit 2.0, ThermoFisher Scientific, USA). 100 µg of the protein sample was reduced with 6 mM TCEP (final) at 37 °C for 10 minutes, then alkylated with 20 mM acrylamide (final) at room temperature for 20 minutes. The protein was then digested with 2 µg trypsin (Trypsin Gold, Promega) overnight at 37 °C in the filter. Peptides were separated from undigested protein by centrifugation (14,000 *g* × 20 minutes) and acidified with 1% formic acid (final) and centrifuged (10,000 *g* × 2 minutes) to remove deoxycholate. Peptides were then desalted with C18 tips (Omix Bond Elut, Agilent Technologies), dried by vacuum centrifugation, and stored at 4 °C until analysis.

Mass spectrometry

Peptides were resuspended in 0.1% formic acid, dissolved at 37 °C for 30 minutes, and analysed by liquid chromatography-tandem mass spectrometry. Samples of 250 ng total peptide were loaded onto an Acclaim PepMap C18, 50 cm, 75 µm inner diameter, 3 µm particle size, 100 Å column (#164570, ThermoFisher Scientific) and Ultimate 3000 liquid chromatograph (ThermoFisher Scientific). Peptides were eluted by a 120-minute gradient from 3%–35% buffer B (buffer A: 0.1% formic acid; buffer B: 80% acetonitrile, 0.1% formic acid) at 300 nL min^{-1}

and 55 °C. Peptides were analysed with a Lumos Tribrid Hybrid mass spectrometer (ThermoFisher Scientific) by electrospray ionisation at a 1.8 kV spray voltage and a resolution of 120,000. The top 20 MS peaks over a scan range of 375–1400 m/z were analysed by the orbitrap, rejecting +1 charge states and with dynamic exclusion enabled (60 s). Peptides were fragmented by collision-induced dissociation and fragments analysed by the ion trap. The instruments were operated with Chromeleon (v7.3.1), Xcalibur (v4.7), and Tune (v4.1.4244) (ThermoFisher Scientific).

Protein identification was conducted using the Andromeda search engine in MaxQuant (v2.2) against protein models derived from the *Exaiptasia diaphana* genome [34] or *Breviolum minutum* transcriptome [70]. False discovery rate (FDR) thresholds were set at 1% for peptide and protein search matches, and a minimum of two peptides per protein were required for identification. Searches assumed trypsin digestion with a maximum of two missed cleavages [46]. Oxidation of methionine and acetylation of the protein N-terminus were specified as variable modifications, and carbamidomethylation of cysteine was specified as a fixed modification. The 'match between runs' feature was enabled, and peptide-sequence matches were grouped by parsimony and quantified by label-free quantification intensity.

Protein abundance analysis

Protein abundance analysis was as per [46] where all known false matches were removed and all protein label-free quantification intensity values were $\log_2$- transformed. Differentially abundant proteins (DAPs) were then identified using Limma [71] based of a FDR <0.1 and Log_2-FC of >0.25 or <-0.25. SODs (superoxide dismutase) identified from the proteomics were also analysed due to their known link with Mn and antioxidant activities.

Cell counts

Cell counts of Symbiodiniaceae within individual Aiptasia were performed [46]. Subsamples of homogenised Aiptasia were diluted to 1:10 with ASW and measured via fluorescence microscopy (IN Cell 6500 HS; GE Health-care, Sydney Australia, ex. 642 nm), and cells were quantified using IN Carta software (GE Life Science) (n = 6). Total cell counts were then normalised to host protein content to give cells per µg of protein.

Statistical analysis

All statistical tests (One Way and Two Way Analysis of Variance (ANOVA), Tukey post-hoc, Individual t tests, Pearsons, Shapiro-Wilk, Levene's and Non-parametric Kruskal-Wallis test) were conducted in R-Studio (Boston, MA). Principal Component Analysis (PCA) plots (Fig. 2a, b) and PERMANOVAs were conducted using Metaboanalyst 5.0 (Canada) incorporating all detected proteins using cube root data transformation and auto scaling. Finally, PANNZER2 [72] was used to annotate identified proteins with GO terms by sequence homology. Gene Ontology (GO) term enrichment was then performed using the package topGO (v. 2.56.0, Alexa et al. 2024) in R (v. 12.0 (R Core Team 2021). GO terms of DAP's (FDR < 0.1) between specific treatments were tested for enrichment ($p < 0.1$) using Fisher's exact test with a node size of 2.

Author contributions

HE and EFC conceived the project with input from DH, JM and AH. HE conducted the experiment. HE and CO undertook the proteomics analysis. KS conducted Top GO analysis. EFC, JM, and AH supervised the project. HE and EFC led the writing, with input and editing from all. EFC acquired the funding and administered the project.

Acknowledgments

Funding of this work was supported from a Philanthropic Donation of David and Susan Rockefeller to EFC.

Data availability

The authors declare that data supporting the findings of this study are available within the paper, Supplementary Materials and Supplementary Data. Proteomics data is available online at https://doi.org/10.5281/zenodo.18398778 under the repository name 'England et al. 2026 Comms Bio'

Competing interests

All authors declare no competing interests.

References

1. Ferrier-Pagès, C., Schoelzke, V., Jaubert, J., Muscatine, L. & Hoegh-Guldberg, O. Response of a scleractinian coral, *Stylophora pistillata*, to iron and nitrate enrichment. *J. Exp. Mar. Biol. Ecol.* **259**, 249–261 (2001).
2. Pogoreutz, C. *et al.* Coral holobiont cues prime Endozoicomonas for a symbiotic lifestyle. *ISME J.* **16**, 1883–1895 (2022).
3. LaJeunesse, T. C. *et al.* Systematic Revision of Symbiodiniaceae Highlights the Antiquity and Diversity of Coral Endosymbionts. *Curr. Biol.* **28**, 2570-2580.e6 (2018).
4. Grima, A. J. *et al.* Species-specific elementomes for scleractinian coral hosts and their associated Symbiodiniaceae. *Coral Reefs* **41**, 1115–1130 (2022).
5. Hillyer, K. E. *et al.* Metabolite profiling of symbiont and host during thermal stress and bleaching in the coral Acropora aspera. *Coral Reefs* **36**, 105–118 (2017).
6. Matthews, J. L. *et al.* Partner switching and metabolic flux in a model cnidarian–dinoflagellate symbiosis. *Proc. R. Soc. B Biol. Sci.* **285**, 20182336 (2018).
7. Ros, M. *et al.* Unlocking the black-box of inorganic carbon-uptake and utilization strategies among coral endosymbionts (Symbiodiniaceae). *Limnol. Oceanogr.* **65**, 1747–1763 (2020).
8. Nielsen, D. A., Petrou, K. & Gates, R. D. Coral bleaching from a single cell perspective. *ISME J.* **12**, 1558–1567 (2018).
9. Yellowlees, D., Rees, T. A. V. & Leggat, W. Metabolic interactions between algal symbionts and invertebrate hosts. *Plant Cell Environ.* **31**, 679–694 (2008).
10. Suggett, D. J. & Smith, D. J. Coral bleaching patterns are the outcome of complex biological and environmental networking. *Glob. Change Biol.* **26**, 68–79 (2020).

11. Rädecker, N. *et al.* Heat stress destabilizes symbiotic nutrient cycling in corals. *Proc. Natl. Acad. Sci.* **118**, e2022653118 (2021).
12. Hughes, T. P. *et al.* Global warming and recurrent mass bleaching of corals. *Nature* **543**, 373-377H (2017).
13. Montalbetti, E. *et al.* Manganese Benefits Heat-Stressed Corals at the Cellular Level. *Front. Mar. Sci.* https://doi.org/10.3389/fmars.2021.681119 (2021) doi:10.3389/fmars.2021.681119.
14. Biscéré, T., Ferrier-Pagès, C., Gilbert, A., Pichler, T. & Houlbrèque, F. Evidence for mitigation of coral bleaching by manganese. *Sci. Rep. Nat. Publ. Group* **8**, 1–10 (2018).
15. Camp, E. F. *et al.* Micronutrient content drives elementome variability amongst the Symbiodiniaceae. *BMC Plant Biol.* **22**, 184 (2022).
16. Reich, H. G., Camp, E. F., Roger, L. M. & Putnam, H. M. The trace metal economy of the coral holobiont: supplies, demands and exchanges. *Biol. Rev.* **98**, 623–642 (2023).
17. Balaguer, J., Koch, F., Hassler, C. & Trimborn, S. Iron and manganese co-limit the growth of two phytoplankton groups dominant at two locations of the Drake Passage. *Commun. Biol.* **5**, 1–12 (2022).
18. Browning, T. J., Achterberg, E. P., Engel, A. & Mawji, E. Manganese co-limitation of phytoplankton growth and major nutrient drawdown in the Southern Ocean. *Nat. Commun.* **12**, 884 (2021).
19. Holley, A. K., Bakthavatchalu, V., Velez-Roman, J. M. & St. Clair, D. K. Manganese Superoxide Dismutase: Guardian of the Powerhouse. *Int. J. Mol. Sci.* **12**, 7114–7162 (2011).
20. Schmidt, S. B. *et al.* Photosystem II Functionality in Barley Responds Dynamically to Changes in Leaf Manganese Status. *Front. Plant Sci.* **7**, (2016).

21. Banci, L. Structural properties of peroxidases. *J. Biotechnol.* **53**, 253–263 (1997).

22. Wilcox, S. K. *et al.* Rational Design of a Functional Metalloenzyme: Introduction of a Site for Manganese Binding and Oxidation into a Heme Peroxidase. *Biochemistry* **37**, 16853–16862 (1998).

23. Dykens, J. A. & Shick, J. M. Oxygen production by endosymbiotic algae controls superoxide dismutase activity in their animal host. *Nature* **297**, 579–580 (1982).

24. Grasso, L. C. *et al.* Microarray analysis identifies candidate genes for key roles in coral development. *BMC Genomics* **9**, 540 (2008).

25. Golding, L. A. *et al.* Acute and chronic toxicity of manganese to tropical adult coral (*Acropora millepora*) to support the derivation of marine manganese water quality guideline values. *Mar. Pollut. Bull.* **194**, 115242 (2023).

26. Morley, N. H., Burton, J. D., Tankere, S. P. C. & Martin, J.-M. Distribution and behaviour of some dissolved trace metals in the western Mediterranean Sea. *Deep Sea Res. Part II Top. Stud. Oceanogr.* **44**, 675–691 (1997).

27. Srichandan, S. *et al.* Distribution of trace metals in surface seawater and zooplankton of the Bay of Bengal, off Rushikulya estuary, East Coast of India. *Mar. Pollut. Bull.* **111**, 468–475 (2016).

28. S, R. R. *et al.* Heavy Metal Contamination and Risk Assessment in the Marine Environment of Arabian Sea, along the Southwest Coast of India. *Am. J. Chem.* **2**, 191–208 (2012).

29. Summer, K., Reichelt-Brushett, A. & Howe, P. Toxicity of manganese to various life stages of selected marine cnidarian species. *Ecotoxicol. Environ. Saf.* **167**, 83–94 (2019).

30. England, H. *et al.* Timing and method of manganese supplementation effects thermal resilience of Acropora millepora. *BioMetals* https://doi.org/10.1007/s10534-025-00774-7 (2025) doi:10.1007/s10534-025-00774-7.

31. Dungan, A. M. *et al.* Exaiptasia diaphana from the great barrier reef: a valuable resource for coral symbiosis research. *Symbiosis* **80**, 195–206 (2020).

32. Matthews, J. L. *et al.* Menthol-induced bleaching rapidly and effectively provides experimental aposymbiotic sea anemones (Aiptasia sp.) for symbiosis investigations. *J. Exp. Biol.* **219**, 306–310 (2016).

33. Matthews, J. L. *et al.* Optimal nutrient exchange and immune responses operate in partner specificity in the cnidarian-dinoflagellate symbiosis. *Proc. Natl. Acad. Sci.* **114**, 13194–13199 (2017).

34. Baumgarten, S. *et al.* The genome of Aiptasia, a sea anemone model for coral symbiosis. *Proc. Natl. Acad. Sci.* **112**, 11893–11898 (2015).

35. Lehnert, E. M., Burriesci, M. S. & Pringle, J. R. Developing the anemone Aiptasia as a tractable model for cnidarian-dinoflagellate symbiosis: the transcriptome of aposymbiotic A. pallida. *BMC Genomics* **13**, 271 (2012).

36. Sproles, A. E. *et al.* Proteomics quantifies protein expression changes in a model cnidarian colonised by a thermally tolerant but suboptimal symbiont. *ISME J.* **13**, 2334–2345 (2019).

37. Rädecker, N. *et al.* Using Aiptasia as a Model to Study Metabolic Interactions in Cnidarian-Symbiodinium Symbioses. *Front. Physiol.* **9**, (2018).

38. Ferrier-Pagès, C., Sauzéat, L. & Balter, V. Coral bleaching is linked to the capacity of the animal host to supply essential metals to the symbionts. *Glob. Change Biol.* **24**, 3145–3157 (2018).

39. Fujise, L. *et al.* Moderate Thermal Stress Causes Active and Immediate Expulsion of Photosynthetically Damaged Zooxanthellae (Symbiodinium) from Corals. *PLOS ONE* **9**, e114321 (2014).

40. Dasgupta, J., Ananyev, G. M. & Dismukes, G. C. Photoassembly of the Water-Oxidizing Complex in Photosystem II. *Coord. Chem. Rev.* **252**, 347–360 (2008).

41. de Bang, T. C. *et al.* A laser ablation ICP-MS based method for multiplexed immunoblot analysis: applications to manganese-dependent protein dynamics of photosystem II in barley (Hordeum vulgare L.). *Plant J.* **83**, 555–565 (2015).

42. Smythers, A. L. *et al.* Excess manganese increases photosynthetic activity via enhanced reducing center and antenna plasticity in Chlorella vulgaris. *Sci. Rep. Nat. Publ. Group* **13**, 11301 (2023).

43. Allakhverdiev, S. I. *et al.* Heat stress: an overview of molecular responses in photosynthesis. *Photosynth. Res.* **98**, 541–50 (2008).

44. Mathur, S., Agrawal, D. & Jajoo, A. Photosynthesis: Response to high temperature stress. *J. Photochem. Photobiol. B* **137**, 116–126 (2014).

45. Iyagbaye, L., Reichelt-Brushett, A. & Benkendorff, K. Manganese uptake and partitioning between the tissue of the anemone host *Exaiptasia pallida* and *Symbiodinium* spp., including assessment of stress and recovery. *Chemosphere* **295**, 133895 (2022).

46. Oakley, C. A., Newson, G. I., Peng, L. & Davy, S. K. The Symbiodinium Proteome Response to Thermal and Nutrient Stresses. *Plant Cell Physiol.* **64**, 433–447 (2023).

47. Crystal Structure of the Oxygen-Evolving Complex of Photosystem II | Inorganic Chemistry. https://pubs-acs-org.ezproxy.lib.uts.edu.au/doi/full/10.1021/ic701835r.

48. Guerrero, F. *et al.* A High Redox Potential Form of Cytochrome *c*550 in Photosystem II from *Thermosynechococcus elongatus**. *J. Biol. Chem.* **286**, 5985–5994 (2011).

49. Roncel, M., Kirilovsky, D., Guerrero, F., Serrano, A. & Ortega, J. M. Photosynthetic cytochrome c550. *Biochim. Biophys. Acta* **1817**, 1152–1163 (2012).

50. Nishiyama, Y., Los, D. A., Hayashi, H. & Murata, N. Thermal protection of the oxygen-evolving machinery by PsbU, an extrinsic protein of photosystem II, in Synechococcus species PCC 7002. *Plant Physiol.* **115**, 1473–1480 (1997).

51. Nishiyama, Y., Los, D. A. & Murata, N. PsbU, a protein associated with photosystem II, is required for the acquisition of cellular thermotolerance in Synechococcus species PCC 7002. *Plant Physiol.* **120**, 301 (1999).

52. Roose, J. L., Frankel, L. K., Mummadisetti, M. P. & Bricker, T. M. The extrinsic proteins of photosystem II: update. *Planta Int. J. Plant Biol.* **243**, 889–908 (2016).

53. Nagao, R. *et al.* Binding and Functional Properties of Five Extrinsic Proteins in Oxygen-evolving Photosystem II from a Marine Centric Diatom, Chaetoceros gracilis. *J. Biol. Chem.* **285**, 29191–29199 (2010).

54. Chen, M.-C., Cheng, Y.-M., Sung, P.-J., Kuo, C.-E. & Fang, L.-S. Molecular identification of Rab7 (ApRab7) in *Aiptasia pulchella* and its exclusion from phagosomes harboring zooxanthellae. *Biochem. Biophys. Res. Commun.* **308**, 586–595 (2003).

55. Fitt, W. K. & Trench, R. K. Endocytosis of the symbiotic dinoflagellate Symbiodinium microadriaticum freudenthal by endodermal cells of the scyphistomae of Cassiopeia xamachana and resistance of the algae to host digestion. *J. Cell Sci.* **64**, 195–212 (1983).

56. Krueger, T. *et al.* Differential coral bleaching—Contrasting the activity and response of enzymatic antioxidants in symbiotic partners under thermal stress. *Comp. Biochem. Physiol. A. Mol. Integr. Physiol.* **190**, 15–25 (2015).

57. Mukherjee, A. Role of DnaK-DnaJ Proteins in PSII Repair. *Plant Physiol.* **182**, 1804–1805 (2020).

58. Xu, H.-F. *et al.* Dehydration-Induced DnaK2 Chaperone Is Involved in PSII Repair of a Desiccation-Tolerant Cyanobacterium1. *Plant Physiol.* **182**, 1991–2005 (2020).

59. Takahashi, S., Nakamura, T., Sakamizu, M., van Woesik, R. & Yamasaki, H. Repair Machinery of Symbiotic Photosynthesis as the Primary Target of Heat Stress for Reef-Building Corals. *Plant Cell Physiol.* **45**, 251–255 (2004).

60. Yan, Y. *et al.* HSP90.2 promotes CO2 assimilation rate, grain weight and yield in wheat. *Plant Biotechnol. J.* **21**, 1229–1239 (2023).

61. Schlotheuber, M. *et al.* High temporal resolution of hydrogen peroxide (H2O2) dynamics during heat stress does not support a causative role in coral bleaching. *Coral Reefs* **43**, 119–133 (2024).

62. Wang, L. *et al.* The Metabolism of Reactive Oxygen Species and Their Effects on Lipid Biosynthesis of Microalgae. *Int. J. Mol. Sci.* **24**, 11041 (2023).

63. Tolleter, D. *et al.* Coral Bleaching Independent of Photosynthetic Activity. *Curr. Biol.* **23**, 1782–1786 (2013).

64. Dungan, A. M., Maire, J., Perez-Gonzalez, A., Blackall, L. L. & van Oppen, M. J. H. Lack of evidence for the oxidative stress theory of bleaching in the sea anemone, Exaiptasia diaphana, under elevated temperature. *Coral Reefs* **41**, 1161–1172 (2022).

65. Diamant, S., Azem, A., Weiss, C. & Goloubinoff, P. Increased Efficiency of GroE-assisted Protein Folding by Manganese Ions(*). *J. Biol. Chem.* **270**, 28387–28391 (1995).

66. Diamant, S., Azem, A., Weiss, C. & Goloubinoff, P. Effect of free and ATP-bound magnesium and manganese ions on the ATPase activity of chaperonin GroEL14. *Biochemistry* **34**, 273–277 (1995).

67. Chen, P., Bornhorst, J. & Aschner, M. Manganese metabolism in humans. *Front. Biosci. Landmark Ed.* **23**, 1655–1679 (2018).

68. Tsednee, M. *et al.* Manganese co-localizes with calcium and phosphorus in *Chlamydomonas* acidocalcisomes and is mobilized in manganese-deficient conditions. *J. Biol. Chem.* **294**, 17626–17641 (2019).

69. Wisniewski, J. R., Zougman, A., Nagaraj, N. & Mann, M. Universal sample preparation method for proteome analysis. *Nat. Methods* **6**, 359–62 (2009).

70. Parkinson, J. E. *et al.* Gene Expression Variation Resolves Species and Individual Strains among Coral-Associated Dinoflagellates within the Genus Symbiodinium. *Genome Biol. Evol.* **8**, 665–680 (2016).

71. Ritchie, M. E. *et al.* limma powers differential expression analyses for RNA-sequencing and microarray studies. *Nucleic Acids Res.* **43**, e47 (2015).

72. Törönen, P., Medlar, A. & Holm, L. PANNZER2: a rapid functional annotation web server. *Nucleic Acids Res.* **46**, W84–W88 (2018).

Figure 1. Changes in Aiptasia physiology under different levels of manganese (Mn) enrichment and temperature stress. (a) Box plot showing symbiont densities for each treatment (0.5, 4.8, 11.4 and 15.6 µg L^{-1} at 26 and 32ºC) (n = 6) at the end of the experiment.

Whiskers indicating the range of data, the box indicating the interquartile range and solid lines indicating median values. (b) Representative photograph of Aiptasia maintained at 32ºC in 0.5 µg L^{-1} of Mn and (c) Representative photograph of Aiptasia maintained at 32ºC in 15.6 µg L^{-1} of Mn at the end of experiment. (d) Box plots of average maximum quantum yield of PSII (F_v/F_m) values for each treatment at the end of the experiment (*n* = 8). Whiskers indicating the range of data, the box indicating the interquartile range and solid lines indicating median values. (e) Average F_v/F_m values (± SE) for each treatment over the experimental period (*n* = 8). * Indicates significance ($p < 0.05$) between treatments (0.5 µg L^{-1} at 26ºC vs 32ºC (a) ANOVA) and (0.5 µg L^{-1} vs 4.8, 11.4 and 15.6 µg L^{-1} at 32ºC (d) Mann-Whitney U)

Figure 2. Changes in Aiptasia proteomes under different temperatures and manganese (Mn) concentrations. Principal component analysis (PCA) plots for both (a) symbiont and (b) host protein abundances across all treatments. Gradient indicates Mn concentration and colour indicates treatment. (c) Heatmap of differentially abundant proteins (DAPs) (Limma FDR < 0.1, Log_2-Fold change > 0.25, < -0.25) across all treatments for both host and algal symbionts.

Figure 3. Showing differentially abundant proteins (DAP's) and heat shock protein (HSP) abundances between manganese and temperature treatments for Aiptasia symbionts. (a) Changes in the proteome of the algal symbiont *Breviolum minutum* that were significantly different between 0.5 and 15.6 µg L^{-1} at 32ºC (Limma FDR < 0.1, Log_2- Fold change > 0.25, < -0.25). Baseline (dotted line) denotes mean protein abundances for control (0.5 µg L^{-1} at 26º) (n = 4). (b) Volcano plot of all detected proteins between 0.5 and 15.6 µg L^{-1} 32ºC treatments. Significant proteins are coloured purple (Limma FDR <0.1, Log_2- Fold change > 0.25, < -0.25). (c) Fold changes for detected heat shock proteins relevant to control (0.5 µg L^{-1} 26ºC denoted by dashed line) (n = 4).

Figure 4. Superoxide Dismutase abundances across both host and symbionts under different manganese (0.5, 4.8, 11.4 and 15.6µg/ L^{-1}) and thermal treatments (26 and 32ºC) when compared to control (0.5µg/ L^{-1} at 26ºC denoted by dashed line) (n = 4)

Figure 5. Model of Photosystem II (PSII) depicting hypothesised effects of manganese (Mn) limitation (a) and availability (b) on the oxygen evolving complex (OEC) and downstream processes. Mn-limited environment (a1) and Mn-abundant environment (b1). Loss of Mn ions from the Mn cluster due to thermal stress (a2) and replacement of Mn ions (b2). Resulting loss of photosynthetic electron transfer and ultimate inhibition of energy production and downstream cellular processes (a3) as opposed to maintenance of electron transport chain, energy production and cellular functioning (b3). Decreased production of heat shock proteins (HSPs) and increased reactive oxygen species (ROS) generation (a4) and increased production of HSPs and PSII extrinsic proteins (b4). Impaired and damaged extrinsic proteins of the OEC are unable to be repaired/folded (a5). Extrinsic proteins can be repaired as a result of increased HSP production and decreased cellular ROS (b5). Increased cellular abundances of host derived Rab-7a proteins leading to phagocytosis/exocytosis (a6). Symbiont can fend of host derived Rab-7a proteins as a result of maintained cellular functioning and thus leading to the maintenance of cnidarian symbiosis

Editorial summary:

Manganese supplementation at biologically relevant levels enhances cnidarian-dinoflagellate symbiosis in *Exaiptasia daiphana.* mitigating photochemical damage, symbiont loss and revealing mechanistic links in cnidarian thermal tolerance.

Peer review information:

Communications Biology thanks Jin Zhou, Victor H. Beltrán and the other, anonymous, reviewers for their contribution to the peer review of this work. Primary Handling Editors: Linn Hoffmann and Mengtan Xing.

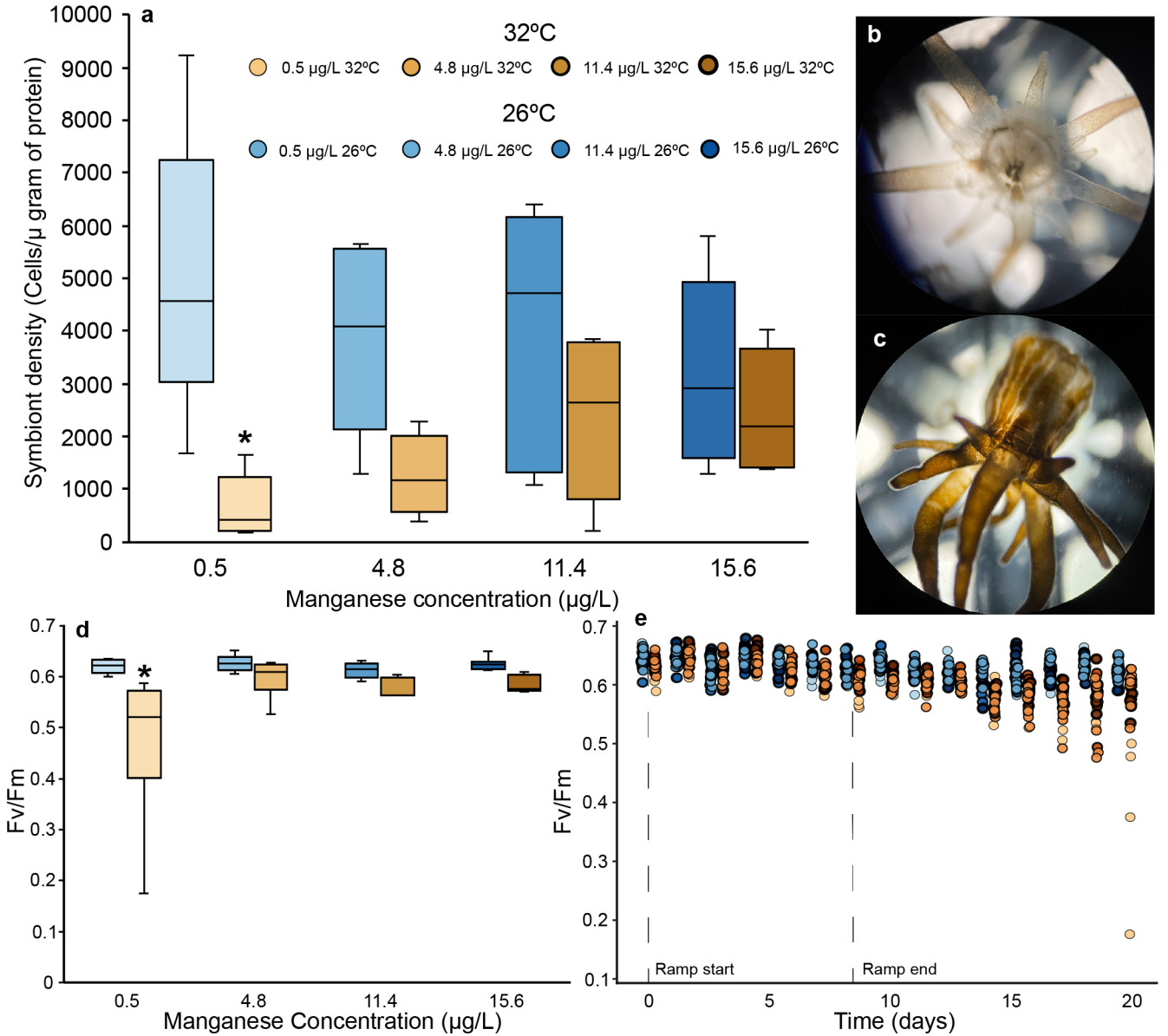
a
32ºC
0.5 µg/L 32ºC
4.8 µg/L 32ºC
11.4 µg/L 32ºC
15.6 µg/L 32ºC
26ºC
0.5 µg/L 26ºC
4.8 µg/L 26ºC
11.4 µg/L 26ºC
15.6 µg/L 26ºC
Symbiont density (Cells/µ gram of protein)
10000
9000
8000
7000
6000
5000
4000
3000
2000
1000
0
*
0.5
4.8
11.4
15.6
Manganese concentration (µg/L)
b
c
d
Fv/Fm
0.7
0.6
0.5
0.4
0.3
0.2
0.1
0
*
0.5
4.8
11.4
15.6
Manganese Concentration (µg/L)
e
Fv/Fm
Ramp start
Ramp end
0
5
10
15
20
Time (days)

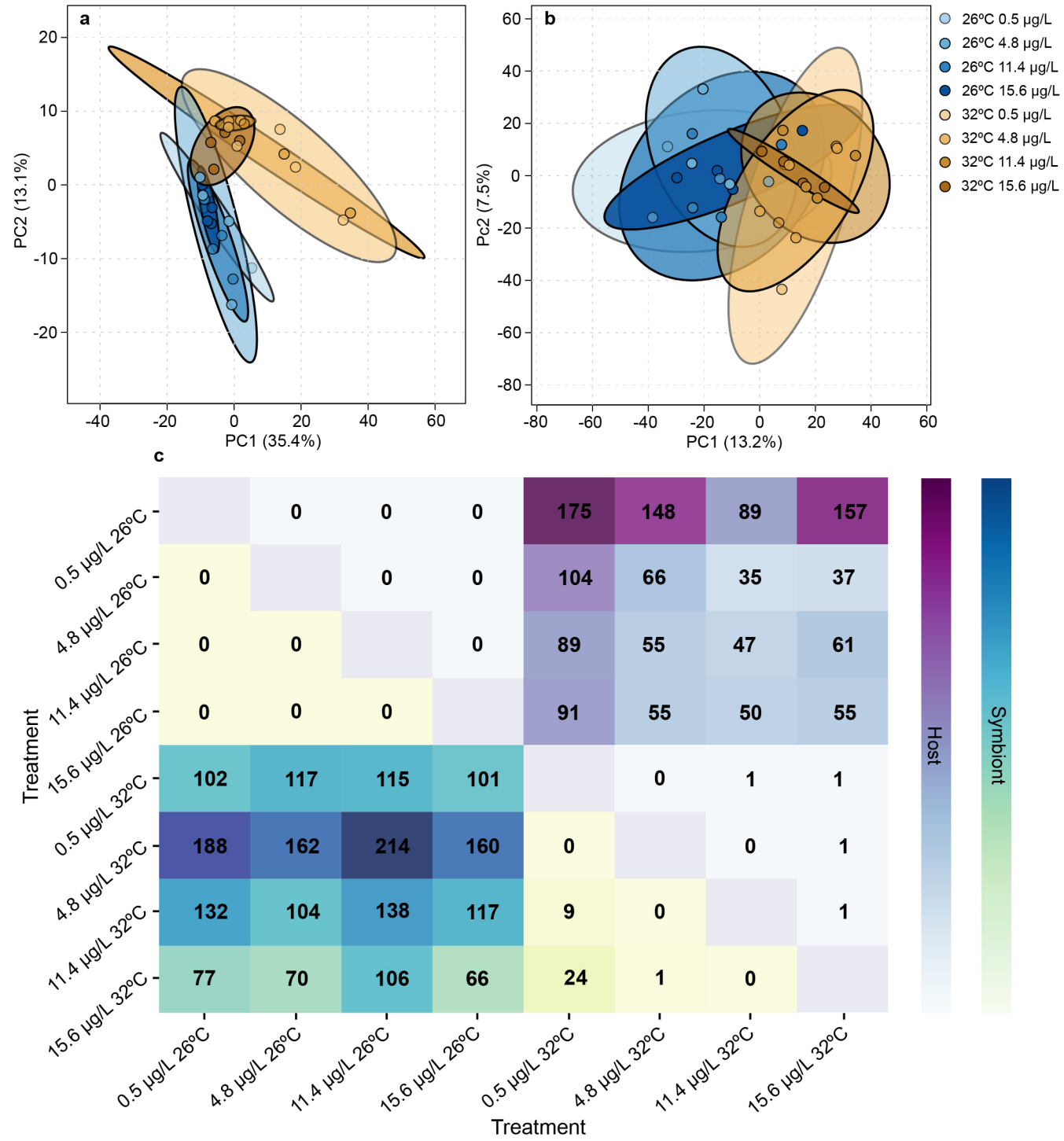
a
PC2 (13.1%)
PC1 (35.4%)
b
Pc2 (7.5%)
PC1 (13.2%)
26ºC 0.5 µg/L
26ºC 4.8 µg/L
26ºC 11.4 µg/L
26ºC 15.6 µg/L
32ºC 0.5 µg/L
32ºC 4.8 µg/L
32ºC 11.4 µg/L
32ºC 15.6 µg/L
c
Treatment
0.5 µg/L 26ºC
4.8 µg/L 26ºC
11.4 µg/L 26ºC
15.6 µg/L 26ºC
0.5 µg/L 32ºC
4.8 µg/L 32ºC
11.4 µg/L 32ºC
15.6 µg/L 32ºC
Host
Symbiont

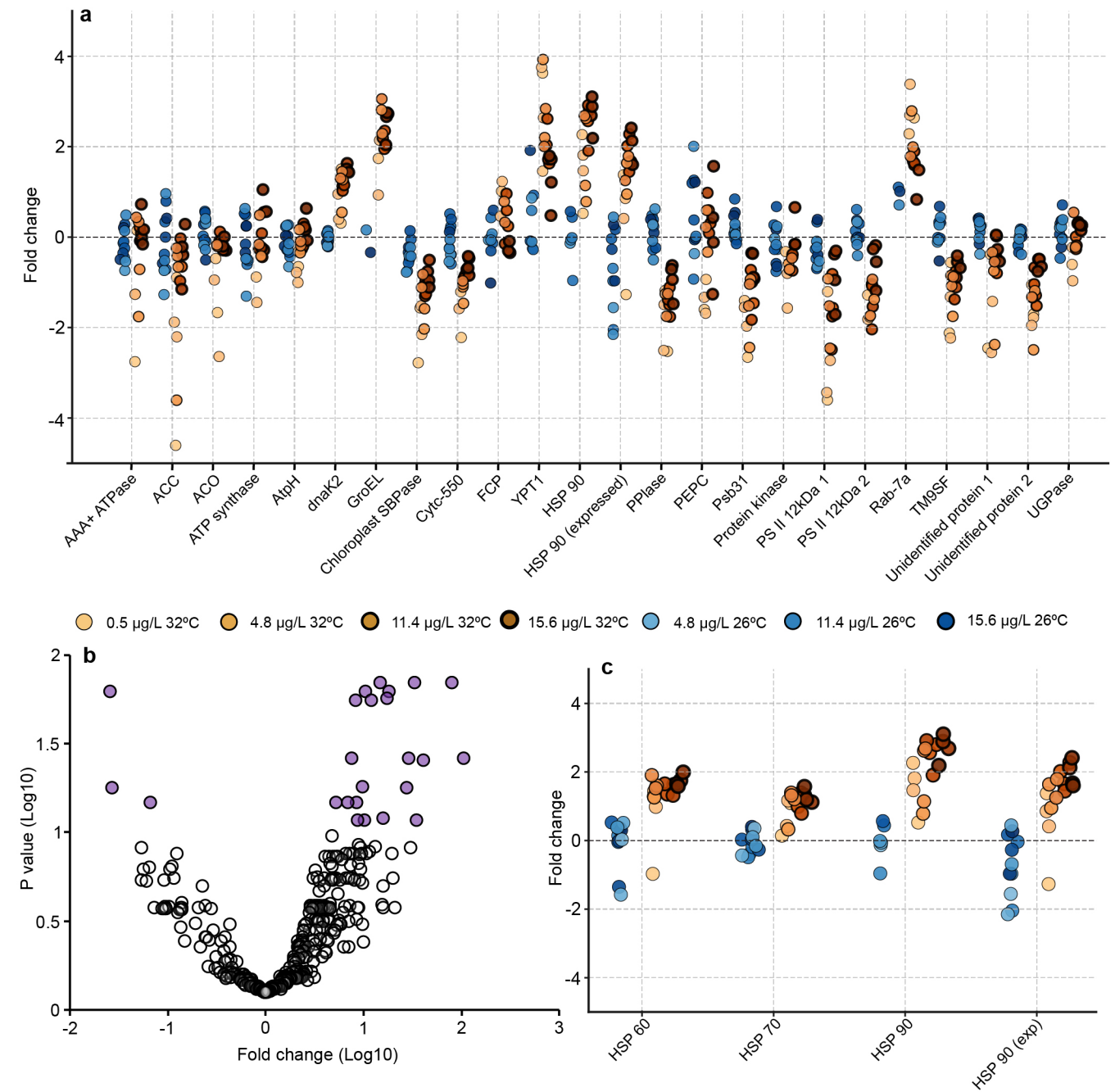
a
Fold change
AAA+ ATPase
ACC
ACO
ATP synthase
AtpH
dnaK2
GroEL
Chloroplast SBPase
Cytc-550
FCP
YPT1
HSP 90
HSP 90 (expressed)
PPIase
PEPC
Psb31
Protein kinase
PS II 12kDa 1
PS II 12kDa 2
Rab-7a
TM9SF
Unidentified protein 1
Unidentified protein 2
UGPase
0.5 µg/L 32ºC
4.8 µg/L 32ºC
11.4 µg/L 32ºC
15.6 µg/L 32ºC
4.8 µg/L 26ºC
11.4 µg/L 26ºC
15.6 µg/L 26ºC
b
P value (Log10)
Fold change (Log10)
c
Fold change
HSP 60
HSP 70
HSP 90
HSP 90 (exp)